

Fluorescence of pyrene-doped polystyrene films from room temperature down to 4 K for wavelength-shifting applications

H. Benmansour^a E. Ellingwood^{a,d} Q. Hars^a P.C.F. Di Stefano^{a,1} D. Gallacher^b M. Kuźniak^c
V. Pereimak^{a,d} J. Anstey^b M.G. Boulay^b B. Cai^b S. Garg^b A. Kemp^{a,d} J. Mason^b
P. Skensved^{a,d} V. Strickland^b M. Stringer^{a,d}

^a*Department of Physics, Engineering Physics & Astronomy, Queen's University, Kingston, ON, K7L 3N6, Canada*

^b*Department of Physics, Carleton University, Ottawa, K1S 5B6, ON, Canada*

^c*AstroCeNT, Nicolaus Copernicus Astronomical Center, Polish Academy of Sciences, Rektorska 4, 00-614 Warsaw, Poland*

^d*Arthur B. McDonald Canadian Astroparticle Physics Research Institute, Queen's University, Kingston ON K7L 3N6, Canada*

E-mail: distefan@queensu.ca

ABSTRACT: In liquid argon-based particle detectors, slow wavelength shifters (WLSs) could be used alongside the common, nanosecond scale, WLS tetraphenyl butadiene (TPB) for background mitigation purposes. At room temperature, pyrene has a moderate fluorescence light yield (LY) and a time constant of the order of hundreds of nanoseconds. In this work, four pyrene-doped polystyrene films with various purities and concentrations were characterized in terms of LY and decay time constants in a range of temperature between 4 K and 300 K under ultraviolet excitation. These films were found to have a LY between 35 and 50% of that of evaporated TPB. All light yields increase when cooling down, while the decays slow down. At room temperature, we observed that pyrene purity is strongly correlated with emission lifetime: highest obtainable purity samples were dominated by decays with emission time constants of ~ 250 – 280 ns, and lower purity samples were dominated by an ~ 80 ns component. One sample was investigated further to better understand the monomer and excimer emissions of pyrene. The excimer-over-monomer intensity ratio decreases when the temperature goes down, with the monomer emission dominating below ~ 87 K.

KEYWORDS: Wavelength shifter, Pyrene, Fluorescence, Liquid argon, Excimer, Monomer

¹Corresponding author.

Contents

1	Introduction	2
2	Wavelength Shifters, Excimers and Monomers	2
3	Equipment and Setup Details	3
3.1	Samples	3
3.2	Time-Resolved Mode	4
3.3	Spectral Mode	6
4	Analysis Techniques	6
4.1	Data Reduction	6
4.2	LED-Induced Noise	6
4.3	SPE Analysis	7
4.4	Fluorescence Yield	8
4.5	Fluorescence Profile Fitting	9
4.5.1	Fits to Full Pulseshape	9
4.5.2	Monomer and Excimer Separation	9
4.6	Spectra	11
5	Results	12
5.1	Temperature Dependent Emission Spectra	12
5.2	Time-Resolved Fluorescence Yield	13
5.3	Fluorescence Decay	13
5.4	Fluorescence Decay Times for Excimer and Monomer Emissions of the P15 Sample	14
5.5	Discussion	16
6	Conclusion	17
7	Acknowledgments	18
A	Calculation of monomer pulse integral	21

1 Introduction

Noble liquids are used as particle detection mediums due to their high scintillation light yields, excellent radio purity capabilities and particle identification abilities. Experiments using noble liquid detectors include direct dark matter detection [1–6], neutrinoless double-beta decay [7], and neutrino observation [8]. In such detectors, a particle interaction in the liquid produces scintillation light roughly proportional to the energy deposited. The vacuum ultra-violet (UV) scintillation emission of liquid argon and xenon (~ 128 nm and ~ 175 nm respectively) make light detection difficult with standard detectors such as photomultipliers (PMs) [9].

One common way to deal with this is to use a wavelength shifter (WLS), a material which absorbs the UV light and re-emits it as easier-to-detect visible light. A standard WLS is 1,1,4,4-tetraphenyl-1,3-butadiene (TPB), characterized by a short, \sim ns, time constant [10], and high conversion efficiency [11]. In certain cases, for instance to identify different regions of the detector [12], it may be advantageous for the WLS to have significantly longer time constants than TPB and argon, enabling a form of spatial pulse-shape discrimination. A similar approach can also be used in liquid scintillator detectors for separation of Cherenkov and scintillation components [13] or other purposes [14].

In this work, we study the fluorescence light yield and decay profiles of four pyrene-doped polystyrene (PS) coatings with diverse pyrene purities and concentrations, excited by a 285 nm LED at temperatures between 4 K and 300 K, including the 87 K boiling point of liquid argon. Fluorescence yield and decay profiles were both determined from time-resolved measurements. One sample was investigated further with spectral measurements to characterize the monomer and excimer responses.

2 Wavelength Shifters, Excimers and Monomers

In particle detectors using noble liquids such as argon, a WLS coating is generally applied between the liquid and the light detectors. WLS are materials that absorb the UV light and re-emit it by fluorescence in the visible spectrum. As noble elements are liquids at low temperatures (87 K for argon), it is important to characterize the WLS in such conditions.

Pyrene ($C_{16}H_{10}$) is a polycyclic aromatic hydrocarbon consisting of four fused benzene rings. Two adjacent molecules of pyrene (monomers) can bond together forming a dimer with an interplanar distance of 3.5 \AA [15]. Both monomers and dimers can be excited; the latter are called excimers. As a pure crystal, pyrene has a high vapor pressure of 6×10^{-6} mbar [16] making it unsuitable for the vacuum requirements of many wavelength-shifting setups. It is therefore often used as a dopant in a more stable matrix of a material like poly(methyl methacrylate) (PMMA, a.k.a. acrylic) [17, 18] or polystyrene (PS) [18]. Room-temperature fluorescence spectra of pyrene in PS films with different pyrene concentrations exhibit two distinct, but broad, emission features, from the monomer (~ 395 nm), and excimer states (~ 470 nm), of pyrene [19]. The amount of excimer emission increases with pyrene concentration [19]. At room temperature, fluorescence decay of diluted monomer happens on a scale of ~ 200 ns [19] — of interest here, since it is significantly slower than TPB and the singlet lifetime of liquid argon.

Fluorescence of pyrene in solid matrices involves three mechanisms [20]. Monomer emission occurs when an isolated pyrene molecule absorbs light, then de-excites radiatively to the ground state. Dynamic excimer emission takes place when an exciton migrates from an excited monomer to a preassociated dimer [21], creating an excimer which de-excites radiatively. Formation of dynamic excimer typically takes place on timescales of nanoseconds or more. Static excimer emission happens when a preassociated dimer is excited, then de-excites radiatively. Due to their proximity, the molecules in the dimer have perturbed absorption and excitation spectra. Static formation takes place on picosecond timescales. Conversion can occur between the processes described above. Mechanisms of monomer and excimer fluorescence are summarized in Fig. 1. While the probabilities of radiative decay do not depend on temperature, temperature dependent non-radiative decays can also take place. The probability of these tends to decrease as temperature falls, contributing to slower decays and generally higher light yields [22].

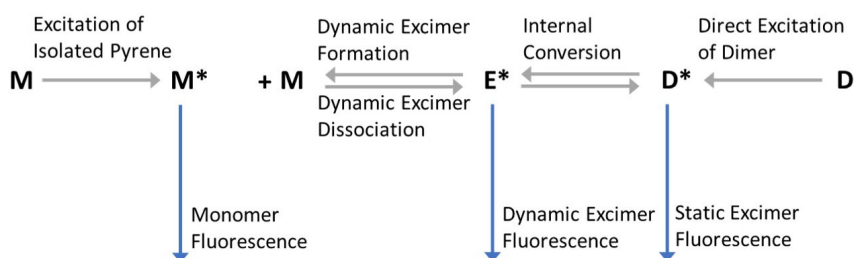


Figure 1. Pyrene fluorescence diagram. M is a ground state pyrene, M* is a pyrene monomer in the first excited state. E* is the dynamic excimer formed by (M*+M), D is the associative ground state pyrene dimer and D* is the dimer in the first excited singlet state. Grey arrows relate to the pyrene molecule processes and blue relate to the fluorescence. Adapted from [20].

3 Equipment and Setup Details

The pyrene fluorescence studies involve data from two different setups. Both feature acrylic substrates coated with pyrene-polystyrene films installed in an optical cryostat [23] to make measurements at temperatures from 300 K down to 4 K under UV excitation. Measurements were taken sequentially while cooling to avoid thermoluminescence, with cross-check measurements performed while warming. Cryostat pressure was $\lesssim 10^{-6}$ mbar.

The time-resolved measurements of the pyrene sample are used to study the fluorescence light yield (number of photons emitted by fluorescence for a given excitation) and decay time of the pyrene coating. This setup features a fast pulsing LED exciting the sample and a PMT to collect the pyrene fluorescence light. The spectral measurement uses the same LED, but with a constant brightness, to excite the sample and a spectrometer to analyze the pyrene fluorescence spectrum.

3.1 Samples

The samples used in this study were made at Carleton University and consist of a pyrene polystyrene mix applied as a film on Reynolds Polymer Technology (RPT) acrylic substrates that were machined

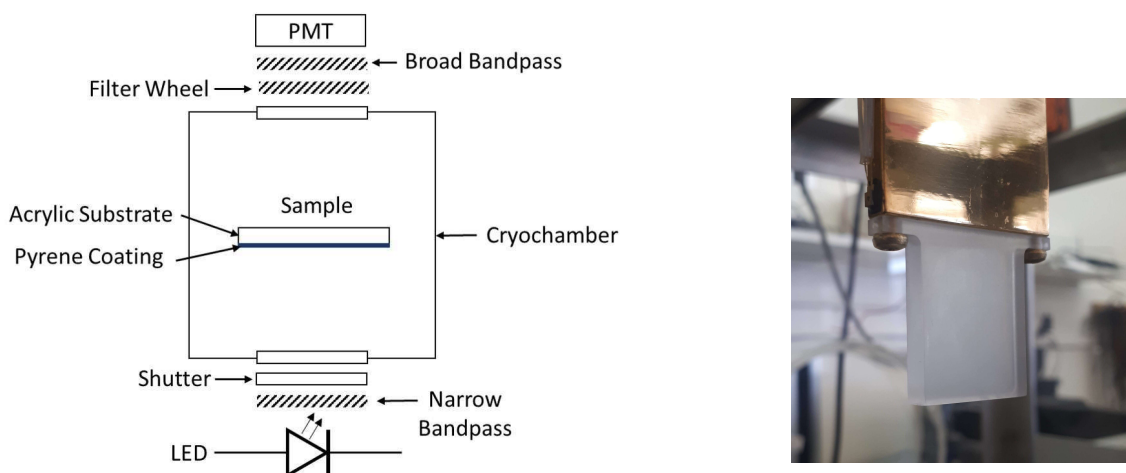


Figure 2. Left: Setup for time-resolved measurements. 285 nm LED light interacts with the pyrene and the acrylic from the sample. The resulting fluorescent light from the sample passes through a filters to select all or parts of the spectrum before being detected on the PMT. Adapted from [24]. Right: Image of an acrylic sample attached to the cold finger of the optical cryostat. The cryostat thermometer is visible on the left side of the cold finger.

to fit in the optical cryostat as shown in Fig. 2. Details of pyrene coating preparation can be found elsewhere [12]. Information on the RPT acrylic can be found in [24].

A total of four different pyrene-polystyrene mixes are studied in this paper. There are three samples with a 15% pyrene concentration by weight (equivalent to $7.78 \times 10^{-4} \text{ mol/cm}^3$) but three different fluorescence grades (98%, 99% and 99.9% purity), called P1598, P1599 and P15 respectively. There is one sample with a 12% pyrene concentration in weight (equivalent to $6.22 \times 10^{-4} \text{ mol/cm}^3$) and a 99.9% fluorescence grade called P12. The pyrene-polystyrene coating was applied on the acrylic substrate with a syringe for P12 and P15, and with a nylon bristled brush for P1598 and P1599.

This report will compare the results from these four samples. An identical substrate coated with evaporated TPB provides a fifth sample for reference. The full analysis of TPB will be presented elsewhere [25].

3.2 Time-Resolved Mode

The setup used for the time-resolved measurements is presented in Fig. 2. The excitation is provided by a 285 nm LED. A function generator produces a 2 V amplitude 50 Hz square wave. This signal is fed into the pulser system which consists of a Kapunstinsky fast-timing pulser circuit [26] that powers the UV LED. This system produces a 285 nm pulse which has a FWHM of ~ 6 ns. Between the LED and the entry window of the cryostat there is a TECHSPEC Hard Coated OD 4.0 10 nm bandpass filter with a central wavelength at 280 nm and a 10 nm FWHM. This filter ensures that the sample is only excited by the wavelength of interest from the LED.

The luminescence of the pulser system can be dependent on the ambient temperature of the room. A W1209 temperature controller was used to stabilize the temperature of this system

by heating it with a resistor attached to the outside of the metal box housing the LED and the Kapustinsky circuit. This kept the circuit and LED at $(29.0 \pm 0.1)^\circ\text{C}$.

The 285 nm LED pulses interact with the pyrene coating producing a distinct fluorescence spectrum with a light yield and pulse decay timing that should depend on the temperature of the sample inside the cryostat. The light then goes through the acrylic substrate, which cuts off any remaining UV component. The optical ordering of UV light, pyrene-doped coating, acrylic, light detection, is similar to that of an argon particle detector like DEAP, made of acrylic, with the inner surface coated with pyrene-doped polystyrene and the light detectors on the other side [12].

The light emitted by the sample passes through the exit window of the cryochamber and then goes through a 660SP Rapid Edge bandpass filter from Omega Optical which accepts light between 375 nm and 660 nm in order to reject any remaining 285 nm LED light. A motorized filter wheel was installed between the UV rejection filter and the PMT to switch between filters that could separate the monomer and excimer components of the pyrene fluorescence emission. The excimer is studied using a Schott GG455 longpass filter with a cut-on wavelength of 455 nm. The monomer part of the spectrum is studied using a Hoya U330 bandpass filter with a 330 nm central wavelength and a 140 nm FWHM. The transmission spectrum for these two filters and the broad bandpass spectrum are shown in Fig. 3.

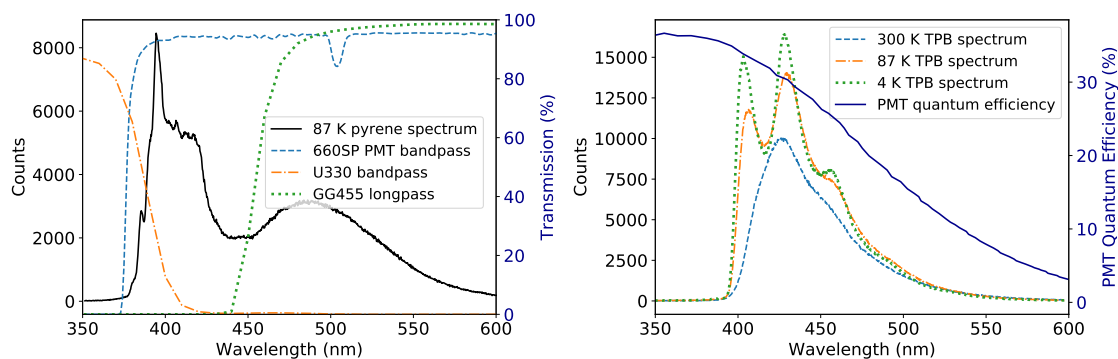


Figure 3. Left: Filters used in time resolved measurements. 660SP Rapid Edge bandpass filter between the cryostat exit window and the PMT, U330 bandpass filter for monomer measurements, GG455 filter for excimer. The P15 spectrum at 87 K with only the PMT bandpass applied is also shown to demonstrate where these filters cut on the spectrum. Right: TPB spectra at multiple temperatures [24], compared to the PMT quantum efficiency, as a function of wavelength [27].

A Hamamatsu R6095-100 photomultiplier tube (PMT) with a super-bialkali photocathode and borosilicate glass is used to collect the fluorescence light from the pyrene which is powered by a CAEN high voltage power supply and recorded using a digitizer. This study uses a National Instruments PXIe-5160 digitizer which has a 10-bit analog input resolution with a 2.5 GS/s sampling rate. The 50 Hz function generator pulse that is fed into the Kapustinsky circuit is also used as the trigger for the digitizer while the PMT output is fed into one of the digitizer channels. The PMT pulse is recorded for $12 \mu\text{s}$ sampled every 0.4 ns. The first $1.2 \mu\text{s}$ of the record are pretrigger. A run at a specified temperature consists of 45 000 of these $12 \mu\text{s}$ events.

3.3 Spectral Mode

The basic setup of this experiment is similar to the time-resolved measurements in its use of the 285 nm LED and the cryostat. The spectra were taken at seven temperatures: 300 K, 250 K, 163 K, 87 K, 77 K, 27 K and 4 K. The two main differences between the time-resolved and spectrometer setup were the LED mode and that the PMT was replaced with a spectrometer. The 285 nm LED was run in DC mode to provide a continuous light source as opposed to a pulsed source. To do this the Kapustinsky circuit was bypassed and the LED was provided with a continuous power input.

This experiment uses a Horiba microHR spectrometer with a Horiba Symphony II liquid-nitrogen cooled open electrode 2D CCD array. The spectrometer and the cryostat are connected via an optical fiber at the same position on the cryostat as the PMT was for the time-resolved measurements. The spectrometer settings, including the filter, wavelength range and exposure, and data acquisition are controlled by the SynerJY program on the DAQ computer. The spectrum window was from 350–650 nm and the exposure was set to 10 s. For each spectrum, an additional exposure with the system shielded from light was subtracted to remove dark counts.

4 Analysis Techniques

4.1 Data Reduction

The digitizer is triggered and synchronized with the LED pulser so there are no spurious pulses in the data set and no cuts have been applied to the data. The data are reduced by two different methods:

- An average pulse is calculated for all the events in a run; the baseline is determined from the pretrigger and subtracted from the average.
- Reduced quantities are calculated for individual pulses; they include the baseline and its sample-by-sample standard deviation, and pulse integral between user-specified bounds.

Data have been analyzed and plotted using the NumPy [28] and Matplotlib [29] python libraries.

4.2 LED-Induced Noise

In all time-resolved measurements, an electronic noise oscillation around the baseline was observed which is due to the pulser circuit. To better understand its characteristics and mitigate its effects, there were dedicated noise runs at at least one temperature, usually 300 K, for each study of a sample. The noise run was taken with an identical procedure to the other time-resolved measurements except that the shutter between the LED and cryochamber was closed. It was then possible to observe noise-only events without the light emitted by the sample.

The red curve in Fig. 4 (top) is an average of the 45 000 noise events. We notice that there is a consistent pattern of fast oscillations with a frequency of several hundreds MHz. This consistency, both in shape and timing, allows us to mitigate the noise by simply subtracting the average pulse shape of a noise-only run from the average shape of any run. The noise and its fluctuations are accounted for in the χ^2 calculation used for pulse fitting as explained in Sec. 4.5.1.

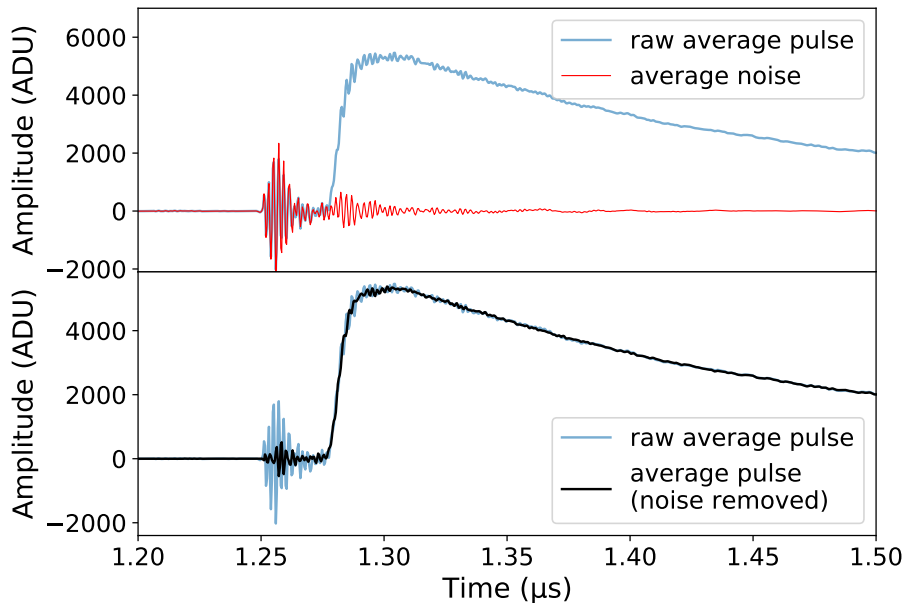


Figure 4. For the analysis, the average noise (red) is removed from the raw average pulse (blue). The average pulse (black) obtained is used to do the fits.

4.3 SPE Analysis

This analysis determines the number of detected photoelectrons as a proxy for light yield. For this, the average single photoelectron (SPE) integral has to be estimated. SPE integral distributions are obtained by reducing the LED voltage to a level where the PMT detects one photoelectron or less for each event. The integration time for each pulse is set to 60 ns. The distribution of these integrals was then fitted with a model describing the photomultiplier response [30], as shown in Fig. 5. This SPE integral distribution corresponds to an empty cryostat configuration, i.e. to the LED barely illuminating the PMT with no sample in between. The reference SPE integral value corresponds to the average integral of a single photoelectron. This property is characteristic of the PMT and high voltage used, and also depends on the vertical range used on the DAQ window.

For this PMT, several SPE runs were carried out with pyrene samples at different temperatures in addition to the empty-cryostat run in Fig. 5. The average SPE integral value was found to be equal to $(13.80 \pm 0.04) \text{ ADU} \cdot \mu\text{s}$, using a vertical range $\pm 0.25 \text{ V}$ for the DAQ. The integral of a given pulse can then be converted into a number of photoelectrons dividing by this SPE integral value.

Lastly, Fig. 5 illustrates the average shape of the LED pulse and PMT response, obtained in the empty cryostat, but with a higher LED intensity to minimize the electronic noise. After normalization, this is used as the instrumental component during pulse deconvolution (Sec. 4.5). Taking this pulse as a proxy for the noisier actual SPE pulses, the shape justifies the 60 ns integration window.

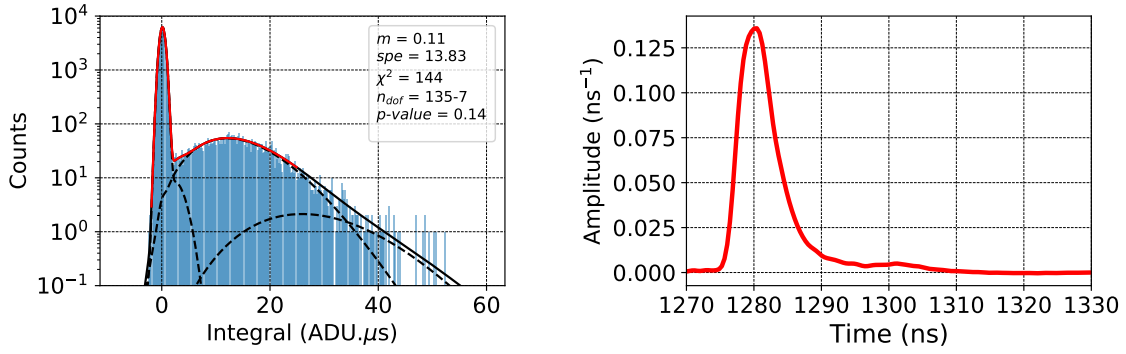


Figure 5. Data obtained with no sample in an empty cryostat. Left: Fitted single photoelectron charge distribution. Average number of photoelectrons per LED pulse is $m = 0.11$; average SPE integral is $13.83 \pm 0.04 \text{ ADU} \cdot \mu\text{s}$. Right: Normalized shape of LED pulse and PM response.

4.4 Fluorescence Yield

To estimate the light yield in each set of conditions, we calculate the integral of each event trace in a run by summing the amplitudes in a given window and weighting by the sampling time. The result is expressed as a number of detected photoelectrons, a proxy for the light yield since the excitation is the same in all runs. A $3 \mu\text{s}$ window is chosen containing more than 99.9% of the overall amount of light, as shown in Fig. 6. This figure also shows the distribution of integrals for all 45 000 events in a run for a pyrene sample at different temperatures.

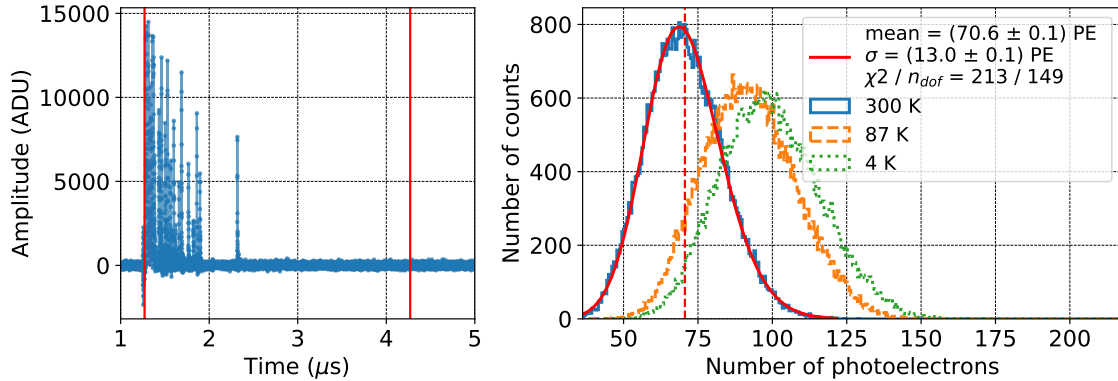


Figure 6. Left: an event from a pyrene run with two red vertical lines (at 1270 ns and 4270 ns) representing the lower and upper limits of the integration window. Individual photoelectrons are clearly visible. Right: event integral distribution for three runs at different temperatures. The blue distribution (300 K) is fitted with a skew normal distribution as an example. The mean of this distribution provided light yield for the sample at that temperature.

The average detected light yield is then obtained by fitting these distributions with a skew normal function [31]. A fit example is shown in Fig. 6. It is carried out by minimizing a Baker-Cousins likelihood [32]. The mean is represented by a vertical dashed red line. The fit of each distribution allows us to calculate the average detected fluorescence yield of the pyrene sample at each temperature. Comparison between temperatures tells us how the absolute light yield changes

with temperature. Using the same method for the TPB sample, we can access the relative light yield of the sample.

4.5 Fluorescence Profile Fitting

One objective of this report is to explore the fluorescence decay times of the four pyrene samples at different temperatures. This requires fitting the average pulse shape with the right physically motivated mathematical model. Fits were carried out in a [1285 ns – 5000 ns] window containing at least 99.9% of the light detected in the event. Fits of the data (d_i photoelectrons at sample i) were carried with a model consisting of the electronic noise (z_i photoelectrons at sample i , determined with the shutter closed as in Sec. 4.2) and the convolved ideal pulse shape (v_i photoelectrons at sample i) as described in the next paragraph. Statistical fluctuations of the number of photoelectrons (standard deviation σ_i) dominate the electronic fluctuations (σ'_i) as seen in Fig. 6. Fits are carried out by minimizing $\chi^2 = \sum_i \frac{(d_i - z_i - v_i)^2}{\sigma_i^2 + \sigma'^2_i}$.

The fluorescence profiles $I(t)$ (in photoelectrons/second) can be modelled by the convolution of the excitation pulse $E(t)$ (in s^{-1}) and the true decay model $i(t)$ (in photoelectrons/second): $I(t) = E(t) * i(t)$. Before fitting, the noise is subtracted from the pyrene average trace in accordance with Sec. 4.2. The excitation pulse $E(t)$ is obtained by having the LED shining on the PMT directly. The pulse obtained then undergoes noise subtraction and is normalized to an integral of 1, see Fig. 5.

4.5.1 Fits to Full Pulseshape

The whole pyrene fluorescence profiles for all four samples were fitted using a sum of three exponentials: two decays and one rise. This ad-hoc model allows us to compare the time constants involved in the various pyrene fluorescence profiles of each sample. The model is presented in Eq. 4.1 with $N_k \geq 0$ and $\tau_k \geq 0$:

$$i(t) = -\frac{N_{rise}}{\tau_{rise}} e^{-\frac{t}{\tau_{rise}}} + \frac{N_1}{\tau_1} e^{-\frac{t}{\tau_1}} + \frac{N_2}{\tau_2} e^{-\frac{t}{\tau_2}} \quad (4.1)$$

A fit using this model on the whole fluorescence profile of P15 at 87 K is shown in Fig. 7. Errors of $\pm 5\%$ were attributed to the values obtained from the fit to account for the systematic and statistical errors from the fit. The contribution to the fluorescence light from the different components can be calculated by integrating the model: $N_{tot} = \int i(t) dt = N_1 + N_2 - N_{rise}$. The fractional contribution of each of the three components is :

$$F_{rise} = \frac{N_{rise}}{N_{tot}} \quad ; \quad F_1 = \frac{N_1}{N_{tot}} \quad ; \quad F_2 = \frac{N_2}{N_{tot}}. \quad (4.2)$$

4.5.2 Monomer and Excimer Separation

The pyrene fluorescence is made of two distinct emissions: monomer and excimer. We have observed them separately using a 330 nm bandpass filter and a 455 nm longpass filter (more details in Sec. 3). A linear combination of them matches the full pulse shape, as shown in Fig. 7 for 87 K. This reconstruction allows us to determine the proportion of monomer and excimer in the total light emitted by the sample at each temperature. To find out the fluorescence decay times, we separately fit the monomer-only and the excimer-only fluorescence profiles.

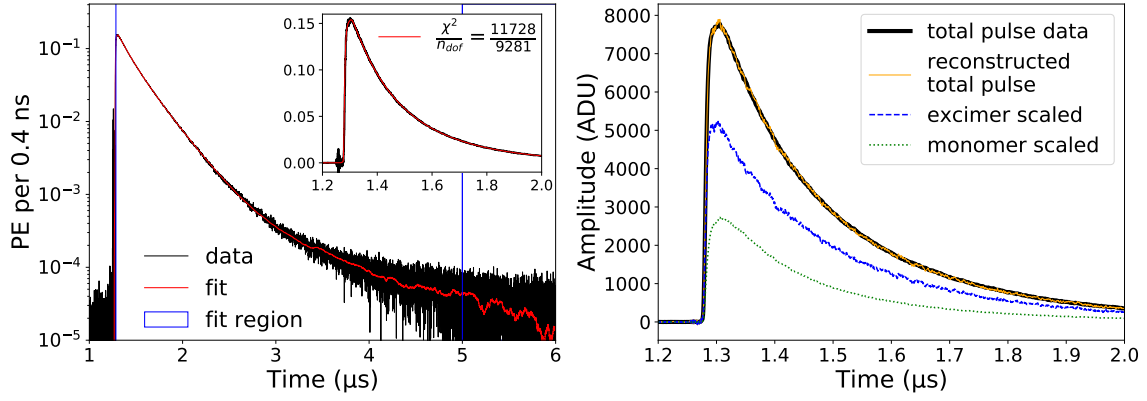


Figure 7. Left: Fit of P15 fluorescence profile at 87 K using Eq. 4.1. (zoom on main feature of pulse and full window in log scale). Right: Pulse reconstruction from monomer and excimer profiles at 87 K. The monomer (green) and excimer (blue) contributions are scaled so that the sum (yellow) is the closest fit to the total pulse data (black).

The unconvoluted monomer profile for pyrene in PS can be described as an exponential decay accelerated by excimer formation [19]:

$$i_m(t) = \frac{N'_1}{\tau'_1} e^{-\frac{t}{\tau'_1} - 2q\sqrt{\frac{t}{\tau'_1}}} \quad (4.3)$$

The first parameter is a decay time τ'_1 corresponding to a pure exponential decay in a dilute monomer system with no excimer formation. The second parameter is dimensionless quantity q , the ratio of the dimer concentration to a critical dimer concentration, itself defined as the concentration at which the rate transfer from excited monomer to excimer is equal to the total rate of excited monomer decay by all other channels. This parameter characterizes the non-exponential nature of the decay caused by excimer formation. Lastly, the total number of photons emitted is $N'_1 \left(1 - qe^{q^2} \sqrt{\pi} [1 - \text{erf}(q)]\right)$ (Appendix A). This model is used to fit the monomer decay in Fig. 8. The decay models for the monomer and excimer are also shown.

For the excimer-only fluorescence, the decay cannot be described by one single exponential; instead we use two decay constants τ'_2 and τ'_3 . In addition, excimer models introduce two populations of excimer: dynamic and static (Sec. 2). A rise time (τ'_{rise}) is included in the model to account for the formation of the dynamic excimer. The model is:

$$i_e(t) = -\frac{N'_{rise}}{\tau'_{rise}} e^{-\frac{t}{\tau'_{rise}}} + \frac{N'_2}{\tau'_2} e^{-\frac{t}{\tau'_2}} + \frac{N'_3}{\tau'_3} e^{-\frac{t}{\tau'_3}} \quad (4.4)$$

The fit shows that at $t = 0$, $i_e \neq 0$, supporting the existence of instantaneous excimer formation, static excimer. The slower rise in the first 20 ns of the pulse indicates the existence of a delayed excimer formation, corresponding to the dynamic excimer.

The contribution to the fluorescence light from the different components can be calculated by integrating the fitting model over the fitting window (Appendix A):

$$F_{monomer} = \frac{N'_m}{N'_{tot}} = \frac{N'_1}{N'_{tot}} \left(1 - qe^{q^2} \sqrt{\pi} (1 - \text{erf}(q))\right) \quad (4.5)$$

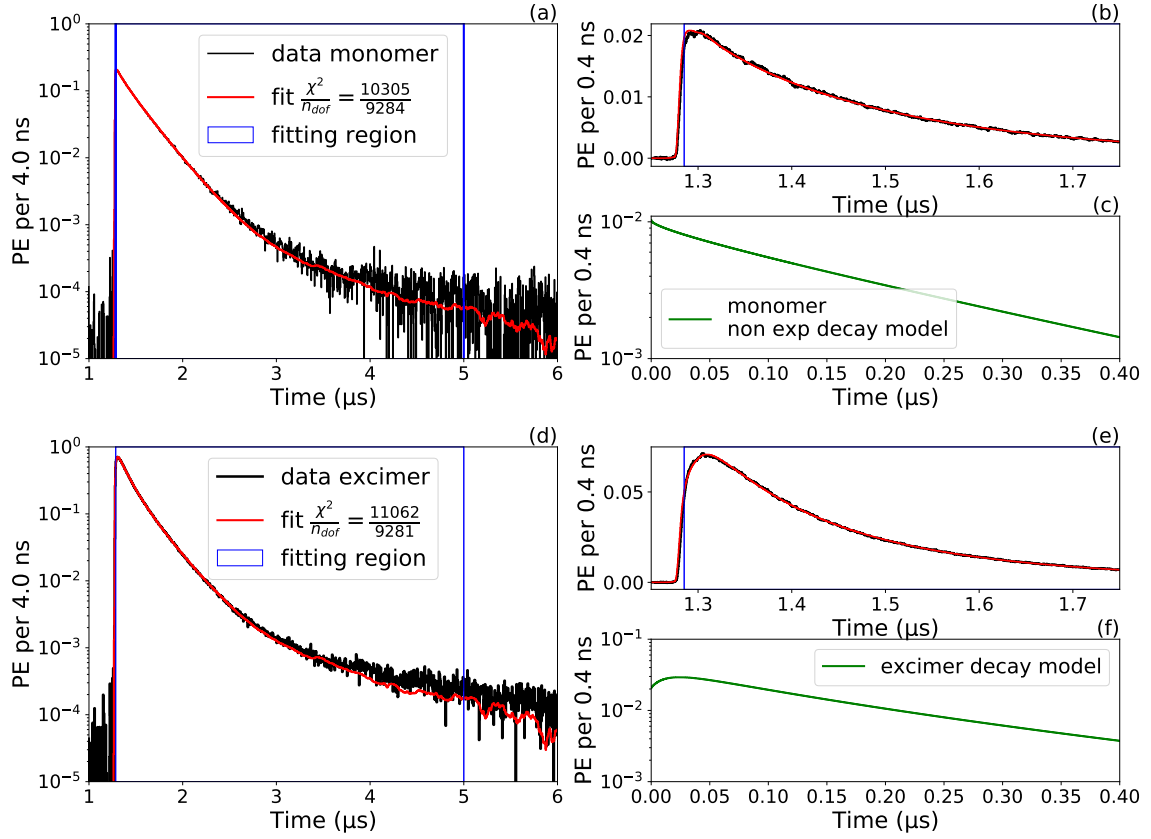


Figure 8. (a): Monomer fit to 87 K data on the full fit window in log scale using the model presented in Eq. 4.3. (b): Zoom on fit. (c): and monomer decay model. Bottom three figures (d), (e) and (f) are the same, but for excimer. Excimer decay model shows a non-zero initial value corresponding to static excimer, and a subsequent rise, corresponding to dynamic excimer.

$$F_{excimer} = \frac{-N'_{rise} + N'_2 + N'_3}{N'_{tot}}, \quad (4.6)$$

with $N'_{tot} = N'_m + N'_2 + N'_3 - N'_{rise}$.

4.6 Spectra

For the spectrometer measurements, the main spectrum was recorded between 350 nm and 650 nm, with 0.3 nm bins. The evolution of the monomer and excimer intensities with temperatures are calculated. No correction was applied to the spectral measurements and the analysis obtained from them. The results are shown in Section 5.1.

5 Results

5.1 Temperature Dependent Emission Spectra

We performed detailed spectral measurements of one sample, P15, to study the contributions of monomer and excimer and their temperature-dependent changes. The spectrum also helps to pick suitable filters to study the monomer and excimer components separately for the time-resolved measurements.

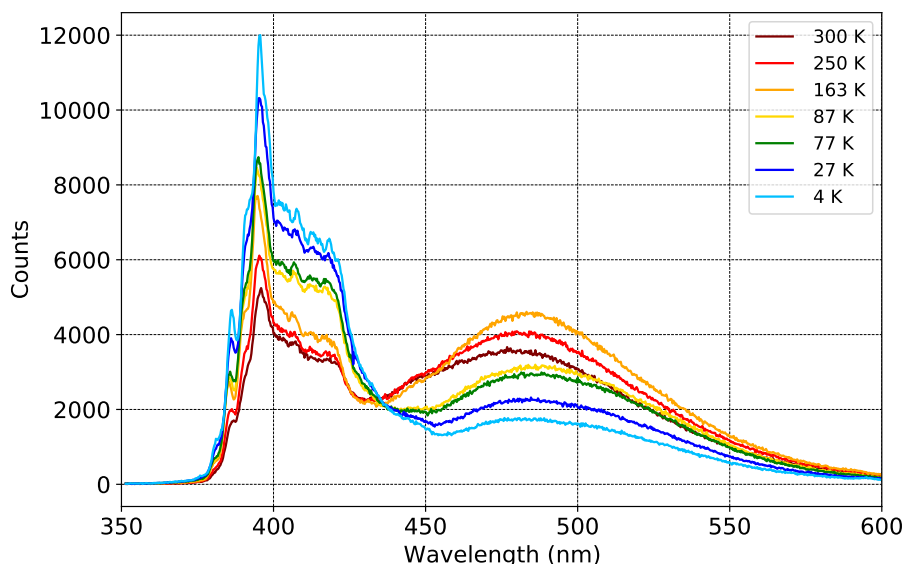


Figure 9. Spectra of P15 at various temperatures. The main monomer spectrum corresponds to the series of peaks below ~ 435 nm while the excimer corresponds to the broad distribution above about ~ 435 nm. The UV-absorbing acrylic substrate explains the sharp drop below 390 nm.

Fig. 9 shows the raw spectra measured using the cryostat and spectrometer for different sample temperatures. The spectra decrease sharply at wavelengths below 390 nm because of absorption from the samples' acrylic substrate. Based on these spectra, the filters to use in the time resolved measurements were chosen to maximize the light yield from the monomer (330 nm bandpass filter) and excimer components (455 nm longpass filter) in wavelength regions where one of the components dominates. Integrated monomer and excimer contributions are shown in Fig. 10. As the temperature decreases, the monomer contribution increases, while the excimer contribution increases at first and then decreases for temperatures below ~ 150 K.

The filters chosen for the time-resolved measurement monomer and excimer study were based on the measured pyrene fluorescence spectrum. The filter transmission spectra are shown in Fig. 3. The 660SP bandpass before the sample is always present during the time-resolved measurements to limit any stray UV LED light from reaching the PMT. To study the whole time-resolved pulse only this filter is present. The monomer is studied using a combination of the U330 bandpass, shown in orange, and the 660SP bandpass. Although the U330 filter cuts out the majority of the peak,

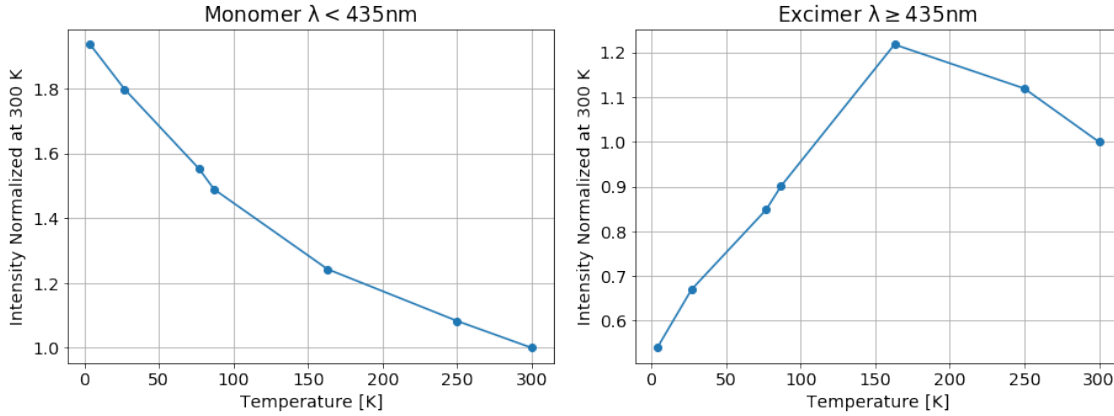


Figure 10. Monomer (left) and excimer (right) intensity obtained from spectrum integration as a function of P15 temperature. Monomer is defined as the region of the spectrum with wavelengths lower than 435 nm and excimer as the region with higher wavelengths. The intensity of the monomer increases with decreasing temperature, while for the excimer, it increases at first with decreasing temperature and then starts to decrease.

the goal was to ensure that the wavelength range limited the broad excimer peak contribution. The excimer is studied using a combination of the GG455 longpass and the 660SP bandpass filters.

5.2 Time-Resolved Fluorescence Yield

The fluorescence yields of four pyrene samples with varying concentrations and purities were studied: P12 (99.9% purity and 12% concentration), P15 (99.9% purity and 15% concentration), P1599 (99% purity and 15% concentration) and P1598 (98% purity and 15% concentration). Using the fits of integral distributions presented in Fig. 6, the number of photoelectrons detected from each pyrene sample is calculated and compared to the number of photoelectrons detected from TPB [25] to provide a proxy of the relative light yield. The result is shown in Fig. 11. The amount of light emitted by all pyrene samples compared to TPB is relatively stable and is between 35% for P1599 at 300 K and 46% for P15 at 4 K. Going from 300 K to 87 K, the relative light yield for P15 increases by 10%.

In the case of sample P15, we can use the monomer and excimer data to correct the light yield for PMT quantum efficiency. The result is overlaid on Fig. 11. This correction increases the relative light yield of P15 with respect to TPB (eg 60% vs 41% at 300 K). The corrected relative light yield falls by 10% when the temperature decreases from 300 K to 87 K.

5.3 Fluorescence Decay

The fluorescence profiles of the four pyrene samples were fitted using the model from Eq. 4.1 in accordance with the method described in Sec. 4.5.1. Fig. 12 gives the values for the two decay time constants τ_1 and τ_2 for temperatures ranging between 4 K and 300 K for four different pyrene samples: P12 (99.9% purity and 12% concentration), P15 (99.9% purity and 15% concentration), P1599 (99% purity and 15% concentration) and P1598 (98% purity and 15% concentration). The contributions F_i from τ_i are defined in Eq. 4.2 (note that $-F_{rise} + F_1 + F_2 = 1$ so $F_1 + F_2 \geq 1$). Because $F_{rise} \leq 4\%$ for all samples at all temperatures, the contribution from the rise component

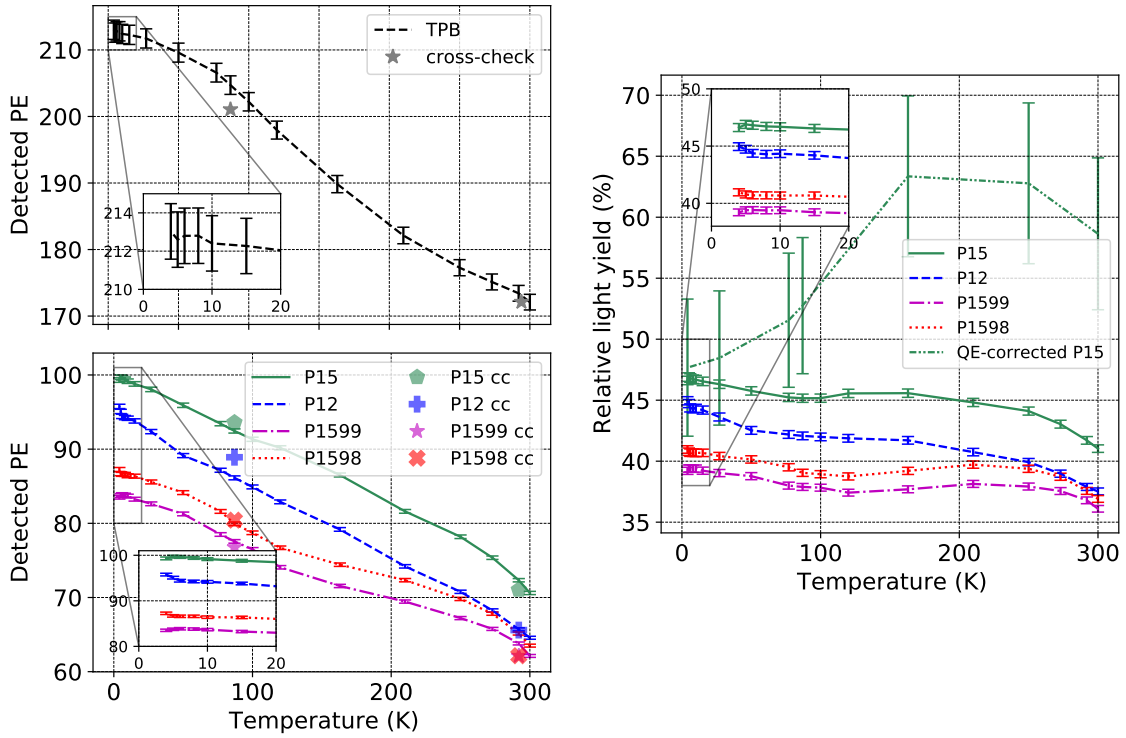


Figure 11. Left: fluorescence yield of the TPB sample (top) and P15, P12, P1599 and P1598 (bottom) expressed as a number of photoelectrons at different temperatures. Results from cross-check (cc) runs at 87 K and room temperature are also shown. Right: fluorescence yield of the pyrene samples relatively to TPB at different temperatures. Quantum efficiency-corrected P15 relative light yield is also displayed.

is negligible compared to the other contributions. This contribution is therefore considered as part of the uncertainty on the other contributions.

From these plots it is clear that the concentration and the purity of pyrene seem to have little influence on τ_1 values at higher temperatures. At lower temperatures, the highest purity samples, P12 and P15, show higher values of τ_1 . The discrepancy is clearer when looking at the longer time constant, τ_2 . Looking at two samples with similar pyrene purities but different pyrene concentrations (P15 and P12), it can be seen that the highest concentration leads to a longer time constant. Looking at three samples with similar pyrene concentrations but different pyrene purities (P15, P1599 and P1598) shows that the highest purity leads to a longer time constant. On the one hand, by comparing P15, P1599 and P1598, it is clear that the lower pyrene purity leads to a much higher contribution from the short time constant τ_1 (70% vs 30% at 300 K). On the other hand, a decreased pyrene concentration leads to a higher contribution from the long time constant τ_2 (80% vs 70% at 300 K).

5.4 Fluorescence Decay Times for Excimer and Monomer Emissions of the P15 Sample

The decay profiles are fitted using the models from Eq. 4.3 and Eq. 4.4 for the monomer and the excimer profiles respectively. Examples of fit are shown in Fig. 8. Fig. 13 plots the evolution of the parameter q from the monomer model and of the three fluorescence decay times: one corresponding

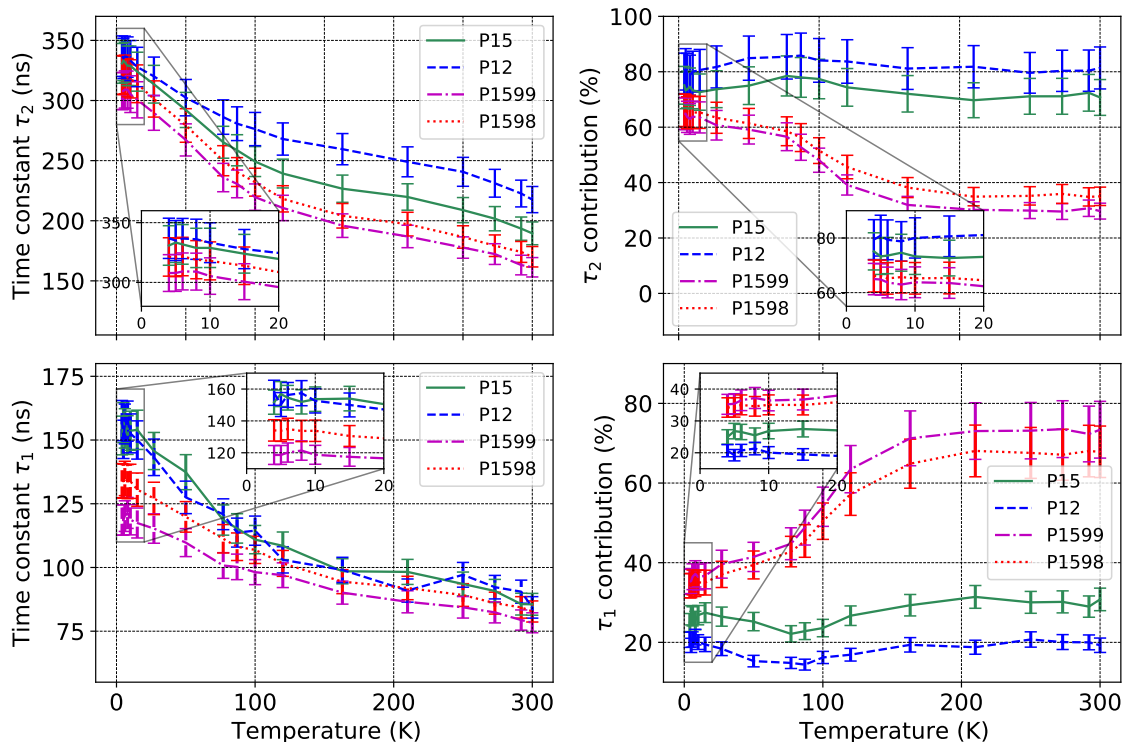


Figure 12. Left: time constants τ_1 and τ_2 for the four different pyrene samples. Right: contribution of each time constant to the light yield.

to the monomer emission, one to the short excimer emission, and one to the long excimer emission. For each component, the contribution to the total light can be determined as a portion of the total light emitted by the sample (Eq. 4.2). As in the previous section, because $F'_{rise} \leq 4\%$ for all samples at all temperatures, the contribution from the rise component is negligible compared to the other contributions. This contribution is therefore considered as part of the uncertainty on the other contributions. The method is described in Sec. 4.5.2.

We notice that τ'_2 is the shortest decay time with values around 100 ns. τ'_2 does not seem to be particularly dependent on the sample temperature. The other decay times all have an increasing trend with decreasing temperature. The evolution of parameter q from Eq. 4.3 is also displayed on Fig. 13. This parameter from the monomer decay model correlates to monomer conversion into excimers [19].

At room temperature, the majority of the light emitted by the sample is due to the excimer emission, but it is equally distributed between the three decay components. When the temperature decreases, the monomer increases its share of the total light while excimer light decreases. At 87 K, the monomer emission represents almost 70% of the the total light. The decay is therefore dominated by a 280 ns component.

As discussed in Sec. 5.2, the PMT QE differs between the monomer and the excimer emission bands. The contribution to the light presented in Fig. 13 can therefore be corrected. The QE-corrected contributions are shown in Fig. 14. As expected, the correction gives more importance

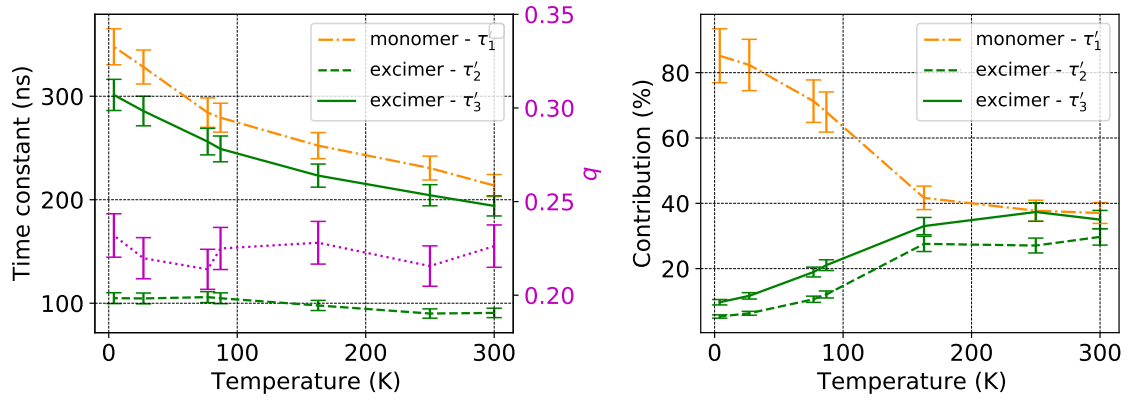


Figure 13. Left: Fluorescence decay times for P15. The monomer profiles are fitted with the model from Eq. 4.3 and the excimer profiles are fitted with model from Eq. 4.4. Parameter q from the model in Eq. 4.3 is also shown. Right: Contribution to the total light from each component of P15 fluorescence decay. Total excimer represents the sum of the short excimer and the long excimer contribution.

to the excimer. The monomer is still the dominant component at 87 K after correction but now contributes 50% of the light at this temperature.

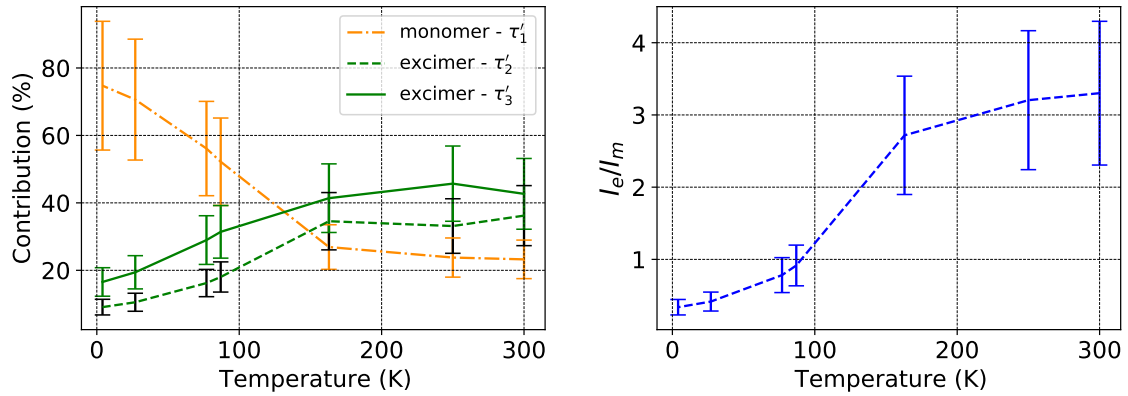


Figure 14. QE-corrected contribution to the total light from each component of P15 fluorescence decay. Total excimer represents the sum of the short excimer and the long excimer contribution. Right: Ratio of the total excimer intensity to the total monomer intensity after PMT QE correction.

5.5 Discussion

Some general trends can be observed in all samples. The light yields of our pyrene samples all increase when temperature goes down (Fig. 11). This has been observed for pyrene in PMMA as well [17]. Overall, we attribute this to the shutting down of non-radiative decay channels. The light yields are between 35% and 50% of TPB at all temperatures (Fig. 11) [25]. Regarding the time constants, all increase during cooling (Fig. 12), consistent with other measurements of pure pyrene crystals [15] and of pyrene in PMMA [17], and also consistent with pyrene in solutions at

higher temperatures [14]. We attribute this as well to the shutting down of non-radiative decay channels during cooling. Fluorescence profiles were fitted with two decay time constants, a short one between 120 ns and 160 ns at 4 K and a long one between 300 ns and 350 ns at the same temperature (Fig. 12). This is generally slower than pyrene in PMMA [17], and significantly slower than the nanosecond timescale of TPB [10, 25].

As for the effect of concentration and purity, at fixed purity, higher concentration leads to higher light yield (Fig. 11). At a fixed concentration of 15%, the highest purity sample (P15) has the highest light yield (Fig. 11). This would be consistent with the main obstacle to fluorescence being quenching impurities. However, the trend is reversed between the P1598 and P1599 samples, possibly because the nominal purities are only lower limits on the purity. The purer pyrenes (P12, P15) tend to have a larger fraction of long decays (Fig. 12). This is consistent with a smaller number of quenching sites from impurities. However, it is important to note that the two least pure samples coatings were applied using a nylon bristled brush while the two other samples films were applied with a syringe. This might contribute to the observed behaviours.

Sample P15 was studied in more detail. As the temperature decreases, the monomer contribution to the light yield increases, whereas that of the excimer increases then decreases (Fig. 10). Previous work on excimers in pyrene crystals down to 100 K [15] shows the same trend. This behaviour is consistent with the first part of cooling being dominated by the reduction in non-radiative decays, and the second part being dominated by a drop in exciton migration, making it harder for dynamic excimer to form. Our excimer-over-monomer intensity ratio decreases when cooling down, as is broadly observed for pyrene in PMMA [17]. Below ~ 100 K, the monomer dominates the emission.

Like the overall time constants, those of the monomer and excimer increase when temperature decreases (Fig. 13). Again, it is consistent with non-radiative decay channels shutting down during cooling. We observe no trend in the behavior of q as a function of temperature (Fig. 13). This is somewhat surprising, as by definition (Sec. 4.5.2), q should depend on non-radiative decay rates. Alternatively, the long, $3.7 \mu\text{s}$, window used in our analysis drowns out the information on q . Lastly, our pulse shapes evidence (Fig. 8) the presence of both static and dynamic excimer [20], respectively forming faster and slower than our time resolution (FWHM of the instrument response in 6 ns).

6 Conclusion

This study considered four pyrene-doped polystyrene coated acrylic samples which had various concentrations and purities of pyrene. The analysis of these samples consisted of a characterization of their fluorescent response to UV light from 300 K to 4 K, in terms of the light yield and decay times. At temperatures from 300 K to 4 K, depending on the pyrene sample, the light yield increased between 30% to 45%. This meant that the relative light yield at 4 K compared to evaporated TPB was at least 40%. The decay profile of pyrene was modelled by two exponential terms: a short decay between 120 ns and 160 ns at 4 K, and a long decay between 300 ns and 350 ns at 4 K. All time constants increased when cooling down and are significantly longer than the nanosecond scale TPB decay. At fixed purity, the highest pyrene concentration sample gave the highest light yield. At fixed concentration, the highest pyrene purity sample gave the highest light yield. The increase

in purity was also found to lead to a higher contribution from the longer time constant decay to the overall decay at all temperatures.

One of the samples was examined in more detail by monitoring the monomer and excimer components separately using filters. The excimer dominates the light yield above ~ 87 K, the monomer dominates below that temperature. The overall behaviour is qualitatively consistent with a reduction in non-radiative channels at low temperature. For the excimer, below 87 K, the results are consistent with a drop in exciton migration.

These pyrene-polystyrene films were developed to act as wavelength shifters with slow time constants and high light yield. When these coatings are placed on specific detector components, these properties of pyrene films can help to provide additional pulse shape discrimination. Such films have been selected by the DEAP collaboration to deal with surface α events in certain regions of the liquid argon detector [12]. Since the surface α background is a limiting background, the ability to discriminate these events increases the discovery potential of the detector. The high light yield and slow decays over the 4–300 K temperature range also makes these pyrene-polystyrene films applicable to background mitigation or event type identification in other liquid argon detectors, in other noble liquid and noble gas-based detectors, and, more generally, in liquid scintillator detectors.

7 Acknowledgments

Funding in Canada has been provided by NSERC through SAPPJ grants, by CFI-LOF and ORF-SIF, and by the McDonald Institute. M.K. is supported by the International Research Agenda Programme AstroCeNT (MAB/2018/7) funded by the Foundation for Polish Science (FNP) from the European Regional Development Fund and by the EU's Horizon 2020 research and innovation program under grant agreement No 962480 (DarkWave). Dr. T. R. Pollmann from NIKHEF and TU München provided comments on a draft of this work. Dr. M. Hamel of CEA Saclay provided insight into the properties of pyrene. Queen's NSERC USRA summer student D. Garrow contributed to the characterization of the instrument response.

References

- [1] DEAP Collaboration. Search for dark matter with a 231-day exposure of liquid argon using DEAP-3600 at SNOLAB. *Physical Review D*, 100(2), Jul 2019.
- [2] DarkSide-50 Collaboration. Results from the first use of low radioactivity argon in a dark matter search. *Physical Review D*, 93(8), Apr 2016.
- [3] XENON1T Collaboration. The XENON1T dark matter experiment. *The European Physical Journal C*, 77(12), Dec 2017.
- [4] LUX Collaboration. The Large Underground Xenon (LUX) experiment. *Nuclear Instruments and Methods in Physics Research Section A: Accelerators, Spectrometers, Detectors and Associated Equipment*, 704:111–126, Mar 2013.
- [5] XMASS-1 Collaboration. Search for inelastic wimp nucleus scattering on ^{129}Xe in data from the XMASS-I experiment. *Progress of Theoretical and Experimental Physics*, 2014(6), 06 2014. 063C01.
- [6] PandaX Collaboration. PandaX: a liquid xenon dark matter experiment at CJPL. *Science China Physics, Mechanics & Astronomy*, 57(8):1476–1494.

- [7] nEXO Collaboration. nEXO: Neutrinoless double beta decay search beyond 10^{28} year half-life sensitivity, 2021. <https://arxiv.org/pdf/2106.16243.pdf>.
- [8] DUNE Collaboration. Volume I. Introduction to DUNE. Journal of Instrumentation, 15(08):T08008–T08008, aug 2020.
- [9] M. Kuźniak and A. M. Szelc. Wavelength shifters for applications in liquid argon detectors. Instruments, 5(1), 2021.
- [10] J.M. Flournoy, I.B. Berlman, B. Rickborn, and R. Harrison. Substituted tetraphenylbutadienes as fast scintillator solutes. Nuclear Instruments and Methods in Physics Research Section A: Accelerators, Spectrometers, Detectors and Associated Equipment, 351(2):349–358, 1994.
- [11] C.H. Lally, G.J. Davies, W.G. Jones, and N.J.T. Smith. UV quantum efficiencies of organic fluors. Nuclear Instruments and Methods in Physics Research Section B: Beam Interactions with Materials and Atoms, 117(4):421–427, October 1996.
- [12] D. Gallacher, A. Leonhardt, H. Benmansour, et al. Development and characterization of a slow wavelength shifting coating for background rejection in liquid argon detectors, 2021. Submitted to Nuclear Instruments and Methods in Physics Research Section A: Accelerators, Spectrometers, Detectors and Associated Equipment, <http://arxiv.org/abs/2109.06819>.
- [13] Steven D. Biller, Edward J. Leming, and Josephine L. Paton. Slow fluors for effective separation of Cherenkov light in liquid scintillators. Nuclear Instruments and Methods in Physics Research Section A: Accelerators, Spectrometers, Detectors and Associated Equipment, 972:164106, 2020.
- [14] M. Hamel et al. Tuning the decay time of liquid scintillators. Journal of Luminescence, 235:118021, 2021.
- [15] J. B. Birks, A. A. Kazzaz, and T. A. King. 'Excimer' Fluorescence. IX. Lifetime Studies of Pyrene Crystals. Proceedings of the Royal Society of London. Series A, Mathematical and Physical Sciences, 291(1427):556–569, 1966.
- [16] W. J. Sonnefeld, W. H. Zoller, and W. E. May. Dynamic coupled-column liquid-chromatographic determination of ambient-temperature vapor pressures of polynuclear aromatic hydrocarbons. Analytical Chemistry, 55(2):275–280, February 1983.
- [17] M. Clark, M. Kuźniak, M. Zheng, and P. Di Stefano. Spectroscopic and time-resolved measurements of the fluorescence of pyrene at low temperatures for noble liquid particle detectors, 2016. Presented at CAP 2016, <https://indico.cern.ch/event/472838/contributions/1150228>.
- [18] A. Itaya et al. Interfacial Characteristics of Poly(methyl methacrylate) Film: Aggregation of Pyrene and Micropolarity Revealed by Time-Resolved Total Internal Reflection Fluorescence Spectroscopy. Polymer Journal, 22(8):697–704, August 1990.
- [19] G. E. Johnson. Effect of Concentration on the Fluorescence Spectra and Lifetimes of Pyrene in Polystyrene Films. Macromolecules, 13:839, 1980.
- [20] F. M. Winnik. Photophysics of preassociated pyrenes in aqueous polymer solutions and in other organized media. Chemical Reviews, 93(2):587–614, 1993.
- [21] J. F. Rabek. Photodegradation of Polymers: Physical Characteristics and Applications. Springer-Verlag Berlin Heidelberg, 1996.
- [22] Y. Takahashi, T. Kitamura, and K. Uchida. Excimer Emission From Evaporated Pyrene Films. Journal of Luminescence, 21(4):425–433, 1980.

- [23] M. A. Verdier et al. A 2.8 K cryogen-free cryostat with compact optical geometry for multiple photon counting. Review of Scientific Instruments, 80(4):046105, 2009.
- [24] J. M. Corning, G. R. Araujo, P. C. F. Di Stefano, V. Pereymak, T. Pollmann, and P. Skensved. Temperature-dependent fluorescence emission spectra of acrylic (PMMA) and tetraphenyl butadiene (TPB) excited with UV light. Journal of Instrumentation, 15(3):C03046, March 2020.
- [25] E. Ellingwood et al. Light yields of tetraphenyl butadiene and RPT acrylic down to 4 K, in preparation. 2021.
- [26] J.S. Kapustinsky et al. A fast timing light pulser for scintillation detectors. Nuclear Instruments and Methods in Physics Research, A241(2-3):612–613, 1985.
- [27] Hamamatsu. Photomultiplier Tubes and Assemblies. https://www.hamamatsu.com/resources/pdf/etd/High_energy_PMT_TPMZ0003E.pdf.
- [28] C. R. Harris et al. Array programming with NumPy. Nature, 585(7825):357–362, September 2020.
- [29] J. D. Hunter. Matplotlib: A 2d graphics environment. Computing in Science & Engineering, 9(3):90–95, 2007.
- [30] I. Chirikov-Zorin, I. Fedorko, A. Menzione, M. Pikna, I. Sýkora, and S. Tokár. Method for precise analysis of the metal package photomultiplier single photoelectron spectra. Nuclear Instruments and Methods in Physics Research Section A: Accelerators, Spectrometers, Detectors and Associated Equipment, 456(3):310–324, 2001.
- [31] R. Cheng. Non-Standard Parametric Statistical Inference. Oxford University Press, 2017.
- [32] S. Baker and R. D. Cousins. Clarification of the use of chi-square and likelihood functions in fits to histograms. Nuclear Instruments and Methods in Physics Research, 221(2):437–442, 1984.

A Calculation of monomer pulse integral

The integral of the non-exponential pulse shape (Eq. 4.5) can be obtained as follows:

$$\begin{aligned}
 \int_0^{+\infty} i_m(t) * E(t) dt &= \frac{N'_1}{\tau'_1} \int_0^{+\infty} e^{-\frac{t}{\tau'_1} - 2q\sqrt{\frac{t}{\tau'_1}}} dt \\
 &= 2N'_1 \int_0^{+\infty} x e^{-x^2 - 2xq} dx \text{ with } x = \sqrt{t/\tau'_1} \\
 &= 2N'_1 \left(\frac{1}{2} - q \int_0^{+\infty} e^{-x^2 - 2xq} dx \right) \text{ integrating by parts} \quad (\text{A.1}) \\
 &= 2N'_1 \left(\frac{1}{2} - q e^{q^2} \int_0^{+\infty} e^{-(x+q)^2} dx \right) \\
 &= N'_1 \left(1 - q e^{q^2} \sqrt{\pi} [1 - \text{erf}(q)] \right) \text{ after } u = x + q
 \end{aligned}$$

where we have used the error function: $\text{erf}(x) = \frac{2}{\sqrt{\pi}} \int_0^x e^{-t^2} dt$